

RESEARCH ARTICLE | SEPTEMBER 06 2024

Optically multiplexed neutron time-of-flight technique for inertial confinement fusion

Special Collection: [Proceedings of the 25th Topical Conference on High-Temperature Plasma Diagnostics](#)

L. Tafoya ; C. Wilde ; B. Cata ; M. Freeman ; V. Geppert-Kleinrath ; S. Ivancic ; J. Katz ; R. McBride ; A. Sorce ; B. Stanley ; C. Danly 

 Check for updates

Rev. Sci. Instrum. 95, 093512 (2024)

<https://doi.org/10.1063/5.0219572>


View
Online


Export
Citation



Optimize
Your
Research

Our Vacuum Gauges Provide
More Process Control
and Operational Reliability



PFEIFFER  VACUUM

Optically multiplexed neutron time-of-flight technique for inertial confinement fusion

Cite as: *Rev. Sci. Instrum.* **95**, 093512 (2024); doi: [10.1063/5.0219572](https://doi.org/10.1063/5.0219572)

Submitted: 17 May 2024 • Accepted: 8 August 2024 •

Published Online: 6 September 2024



View Online



Export Citation



CrossMark

L. Tafoya,^{1,2,a)}  C. Wilde,²  B. Cata,²  M. Freeman,²  V. Geppert-Kleinrath,²  S. Ivancic,³  J. Katz,³ 
R. McBride,¹  A. Sorce,³  B. Stanley,³  and C. Danly² 

AFFILIATIONS

¹ University of Michigan, Ann Arbor, Michigan 48109, USA

² Los Alamos National Laboratory, Los Alamos, New Mexico 87545, USA

³ Laboratory for Laser Energetics, Rochester, New York 14623, USA

Note: This paper is part of the Special Topic on Proceedings of the 25th Topical Conference on High-Temperature Plasma Diagnostics.

^{a)} Author to whom correspondence should be addressed: ltafoya@lanl.gov

ABSTRACT

Neutron time-of-flight (nTOF) detectors are crucial in diagnosing the performance of inertial confinement fusion (ICF) experiments, which implode targets of deuterium–tritium fuel to achieve thermonuclear conditions. These detectors utilize the fusion neutron energy spectrum to extract key measurements, including the hotspot ion temperature and fuel areal density. Previous work [Danly *et al.*, *Rev. Sci. Instrum.* **94**, 043502 (2023)] has demonstrated adding 1D spatial resolution to an nTOF-like detector using a neutron aperture and streak camera to measure the ion temperature profile of an ICF implosion. By contrast, the study presented herein explores modifying the 1D detector to use a fast photomultiplier tube (PMT) to validate the design of a 2D spatially resolved instrument based on reconstruction from 1D profiles. The modification would collect time-of-flight traces from separate scintillators in an imaging array with one PMT using optical fibers of varying lengths to time-multiplex the signals. This technique has been demonstrated in ride-along experiments on the OMEGA laser with 20 fiber-coupled scintillator channels connected to a Photek PMT210. Results provide constraints on the fiber lengths and PMT gating requirements to promote pulse fidelity throughout all channels. Calibration of the detector to fixed nTOFs can provide a preliminary estimate of the instrument response function (IRF), although measurement of the IRF is currently under way. These results suggest that nTOF signals can potentially be time-multiplexed with fibers so long as the design is strategic to mitigate signal-to-noise reduction, modal dispersion, and charge build-up in the PMT, which has implications beyond ion temperature imaging.

© 2024 Author(s). All article content, except where otherwise noted, is licensed under a Creative Commons Attribution (CC BY) license (<https://creativecommons.org/licenses/by/4.0/>). <https://doi.org/10.1063/5.0219572>

I. INTRODUCTION

Laser-driven inertial confinement fusion (ICF) experiments implode spherical capsules filled with hydrogenic isotopes to reach thermonuclear conditions at a central hotspot.^{1,2} The objective of these experiments is to propagate the fusion burn beyond the hotspot through energy deposition from fusion products and incur an ignition instability. However, these implosions are sensitive to HED instabilities and compression asymmetries that can degrade performance and limit the burn.

A primary degradation mechanism is believed to be hotspot contamination, in which high-Z mass from the capsule pusher

or fill-tube is injected into the central hotspot region during compression.^{3,4} Studies suggest that the contaminant mass remains at a lower temperature compared to the surrounding hotspot throughout the burn width of the implosion,⁵ such that the ion temperature distribution can be used to diagnose this mix. The ion temperature is also a fundamental plasma parameter related to fusion reactivity, burn propagation, low-mode asymmetries, and other implosion features. As such, the spatial distribution of the ion temperature within the hotspot contains valuable diagnostic information about the plasma.

The spatially averaged ion temperature can be measured using the energy spectrum of the neutrons emitted in the fusion

reactions.^{6–8} High gain ICF targets utilize a mixture of deuterium and tritium (DT) for the fusion fuel given the high DT reactivity cross section. Each DT reaction emits a characteristic 14.1 MeV neutron, but the neutron emission spectrum is Doppler broadened by the thermal velocity distribution of the parent DT ions in the hotspot. The energy-resolved neutron emission from the implosion can be measured using a time-of-flight detector at a sufficiently far distance to resolve the thermal broadening.

Robust neutron time-of-flight (nTOF) detectors are implemented at ICF facilities, including the OMEGA laser,⁹ the National Ignition Facility (NIF¹⁰), and the Z machine,¹¹ to measure the spatially integrated ion temperature, $\langle T_{ion} \rangle$, fuel areal density, ρR , and several other diagnostic features of the implosion. An nTOF detector generally consists of a fast, neutron-sensitive scintillator coupled to a fast photomultiplier tube (PMT). As the detector samples the total neutron emission along its line-of-sight (LOS), all measured parameters are spatially integrated over the source.

Extensive work has been done on studying the physics underlying the time-of-flight signal to extract measurements of the plasma.¹² The ion temperature can be extracted by forward-fitting the primary DT peak of the detector time signal to a convolution of a fusion neutron energy spectrum (translated to the time-domain) and the instrument response function (IRF) of the detector. The reader is directed to Refs. 12 and 13 for an in-depth discussion of this technique, which is crudely summarized as follows: the detector time signal $F(t)$ can be fit to the following function:

$$F(t) = I(E(t - t_0))s(E(t - t_0))a(E(t - t_0)) \left| \frac{dE}{dt} \right| \otimes R(t), \quad (1)$$

where E is the neutron kinetic energy, I is the neutron spectrum, s is the scintillator energy sensitivity, a describes neutron attenuation along the beamline, and R is the detector IRF. Note that \otimes denotes a time-domain convolution. A single temperature plasma model for the neutron energy spectrum, parameterized in terms of the average ion temperature, is discussed by Ballabio *et al.* in Ref. 7. The scintillator sensitivity s and attenuation a are specific to the detector and line-of-sight and can be measured or estimated using transport simulations. The detector IRF $R(t)$ is generally measured using either

single particle counting or as a convolution of the measured x-ray impulse response and a neutron transport simulation.¹² The form of the IRF is often reasonably described by a Gaussian convolved with some number of exponential decays, each multiplied by a weight factor. A functional form used to describe this can be found in Ref. 14.

II. SPATIALLY RESOLVED NTOF

Spatial resolution can be added to an nTOF-like detector by leveraging techniques developed for the neutron imaging systems (NIS) at the NIF.¹⁵ A 1D spatially resolved ion temperature detector has been previously designed and demonstrated on OMEGA.¹⁶ The instrument utilizes a rolled-edge tungsten slit aperture along with a segmented scintillator array fiber-coupled to a streak camera to collect the measurement. See Ref. 16 for a description of the modeling, capabilities, and first-ever measurement; and Ref. 17 for the instrument design.

Concepts for a 2D spatially resolved detector are currently being investigated and modeled for feasibility. One candidate design would utilize multiple 1D detectors layered along the same diagnostic LOS at distinct angles in order to sample different projections of the neutron emission, which has been projected to the image plane through a neutron aperture. The 1D profiles can then be used to reconstruct a quasi-2D image using few-view tomographic algorithms developed and optimized for neutron imaging.¹⁸ Preliminary reconstructions of NIS images using equally spaced 1D projections with basic back-projection algorithms¹⁹ require ≥ 5 views to resolve spatial features of interest, although an optimized NIS-like algorithm would be expected to produce comparable results with fewer views. A detailed discussion of this technique and the modeling of the diagnostic will be presented in a future publication.

Layering multiple detectors along a given LOS is infeasible in practice if utilizing one streak camera per 1D system, which is consistent with the existing design.¹⁶ The streak camera can, in principle, be replaced by a photomultiplier tube (PMT) if the dimension of spatial-resolution is somehow preserved in the detector scheme. As described in Ref. 16, the scintillators comprising each spatial pixel of the 1D profile are coupled to the streak camera via optical

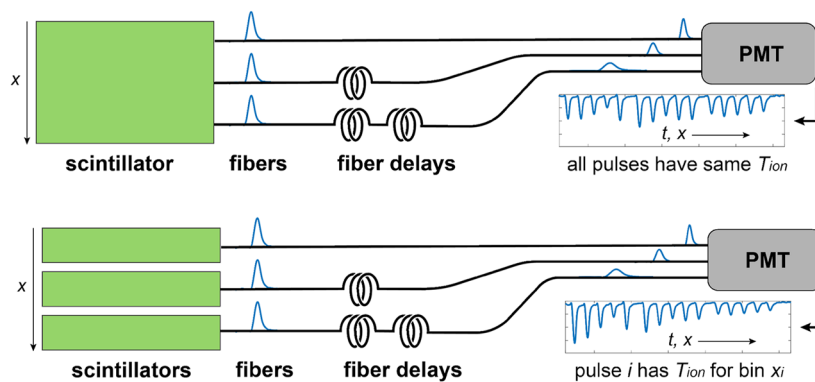


FIG. 1. Concept for time-multiplexing light pulses into a PMT using optical fiber delays to space out the arrival time of different signals. (Top) fibers connected to one scintillator should transmit the same nTOF spectrum and, hence, the same ion temperature (flat-field); and (bottom) each fiber is connected to a separate scintillator (imaging).

fibers. Given that the signal from any given scintillator has a finite transit time through the fiber (~ 5 ns/m for fused-silica²⁰), the total fiber length can be deliberately increased in order to delay the signal arrival time at the detector. Thus, by incrementally increasing the optical fiber length between successive channels by an amount proportional to the width of each scintillation pulse, the signals can be time-multiplexed into a single PMT, encoding the spatial dimension into the time-axis. A diagram illustrating this technique for an nTOF-like detector is shown in Fig. 1. This multiplexing technique is utilized in Doppler velocimetry²¹ and has been proposed for ICF applications.^{12,22}

III. OMEGA PROOF-OF-CONCEPT

To demonstrate the optically multiplexed nTOF technique, a proof-of-concept detector was designed for OMEGA. Typical nTOF spectra from the 13 m LOS (TIM6) were used to calculate the necessary fiber delay lengths to time-multiplex the signals, which should, in principle, work for any distance below 13 m as well. Using an expected neutron pulse width of around 20 ns and pulse separation of around 15 ns, a suitable delay length per channel was estimated to be about 7 m (23 ft) for an average scintillation wavelength of 500 nm. The expected pulse broadening due to modal dispersion is given by the transit time difference between the shortest and longest ray paths in the fiber, which depends on the acceptance angle. For step-index fibers, the time dispersion is then given by $\Delta t = L(n_f/c)(n_f/n_c - 1)$, where n_f is the core index, n_c is the cladding index, and c is the speed of light.²³ Values for the proof-of-concept detector are provided in Table I.

TABLE I. Test multiplexer design parameters. Delay is calculated using an average propagation speed of ~ 5 ns/m (1.5 ns/ft), where the base transit time is 15.75 ns. Attenuation is calculated at the peak emission wavelength of the scintillator (481 nm for EJ-262).

Channel	Length (ft)	Delay (ns)	Attenuation (dB)	Dispersion (ns)
1	10.5	0	0.19	0.52
2	33.5	34.5	0.61	1.66
3	56.5	69.0	1.03	2.80
4	79.5	103.5	1.45	3.93
5	102.5	138.0	1.87	5.07
6	136.5	189.0	2.49	6.75
7	159.5	223.5	2.91	7.89
8	182.5	258.0	3.34	9.03
9	205.5	292.5	3.76	10.16
10	228.5	327.0	4.18	11.30
11	262.5	378.0	4.80	12.98
12	285.5	412.5	5.22	14.12
13	308.5	447.0	5.64	15.26
14	331.5	481.5	6.06	16.39
15	354.5	516.0	6.48	17.53
16	388.5	567.0	7.10	19.22
17	411.5	601.5	7.53	20.35
18	434.5	636.0	7.95	21.50
19	457.5	670.5	8.37	22.63
20	480.5	705.0	8.79	23.77

To verify that fiber-multiplexing does not corrupt the nTOF measurement and determine the limiting delay length before the signal is too heavily degraded, the proof-of-concept detector utilized the same monolithic scintillator for all channels rather than segmented scintillators (the flat-field configuration shown in Fig. 1). The expected result is that all channels should contain the same nTOF trace; thus, after correcting for the instrument response, the same spatially averaged ion temperature should be obtained from each channel. With no need for an aperture, this configuration can be tested as a ride-along experiment on high neutron yield campaigns at OMEGA. Note that a separate array with segmented scintillators for a 1D spatially resolved, multiplexed PMT-based system has recently been tested, but analysis is still ongoing.

Initial 2-channel and 5-channel multiplexing tests were performed with EJ-262 plastic scintillator tiles ($5 \times 1 \times 0.4$ cm³) coupled with 1 mm 0.5NA TCU-1000 PMMA optical fiber to a Photech PMT210 to verify the calculated time-delay separations and probe photon background in the scintillators. These tests validated the calculated fiber delay lengths but showed significant signal attenuation and dispersion with only 5 channels, motivating a switch to fused silica fibers.

A 20-channel multiplexer was then constructed using 400 μ m core 0.37NA silica multi-mode optical fiber (BC-03597-12-BR). The total fiber lengths, pulse delay times, expected attenuation, and expected dispersion are compiled in Table I. The fibers were then coupled into a $20 \times 20 \times 2$ cm³ monolithic piece of EJ-262 plastic scintillator, equally spaced, and inserted along the same edge. Each connection consisted of a cleaved fiber-face inserted into a 1 cm deep bore hole in the scintillator filled with EJ-500 index-matching optical resin. The opposite ends of the fibers were SMA connectorized and inserted into a 3D printed mount to couple to a Photech PMT210. The coupler design was based on the fiber NA to reduce coupling loss, but larger angles of incidence increased window reflections and reduced efficiency. The fiber delays, PMT coupler, and scintillator are shown in Fig. 2. The fiber delays and PMT were

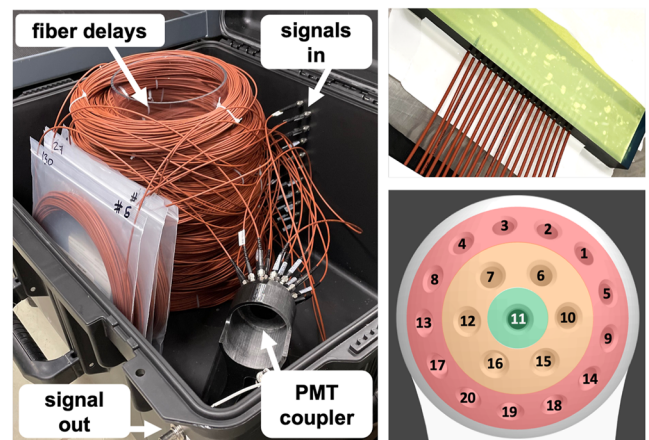


FIG. 2. Test multiplexer hardware design. (Left) fiber-delay spool and PMT coupling bracket in a dark-box; (right-top) fiber-coupled scintillator slab for the flat-field test; and (right-bottom) channel map of fiber coupling to PMT window with 0° offset (green), near 30° offset (yellow), and near 60° offset (red).

kept in a dark-box to isolate the tube from ambient light during operation.

The detector response can, in theory, be estimated using the system photometrics and conversion efficiencies. The number of charge carriers N_e produced by the PMT is given by $N_n \times \epsilon_{int} \times \epsilon_{scint} \times \epsilon_{loss} \times \epsilon_c \times QE \times G$, where N_n is the number of incident neutrons, ϵ_{int} is the fraction that interact in the scintillator, ϵ_{scint} is the scintillation efficiency, ϵ_{loss} is the fiber attenuation, QE is the PMT quantum efficiency, and G is the PMT gain. The remaining term, ϵ_c , describes the coupling efficiency of signal carriers from the scintillator to the photocathode through several non-ideal fiber connections. Determination of this value, however, requires dedicated measurement and calibration, which will be presented in future work.

IV. INITIAL RESULTS AND DISCUSSION

The proof-of-concept multiplexed nTOF (flat-field) has been demonstrated in several campaigns on OMEGA as a ride-along experiment, located both at the lower pylon (port directly below the target chamber, 5 m to the target chamber center) and on the TIM6 LOS. Data collected during the Energetic Neutrons campaign (DT-filled Hoppe-glass targets with an average yield of $\sim 10^{14}$) with the detector positioned at the lower pylon is shown in Fig. 3 and will be the focus of this discussion. As a consequence of the uncollimated and short LOS, fast fusion products and direct interactions in the PMT produce a large signal early in time that corrupts the five shortest fiber channels. However, 15 of the later signals are still well distinguished, as shown in Fig. 3 inset. Note that data have also been collected (in both flat-field and imaging geometries, see Fig. 1) with the detector on the TIM6 LOS, the results of which are consistent with these data but with a significantly less intense background given the further distance (13 m) and collimated LOS. The analysis of the TIM6 data is still ongoing and will be presented in future work.

Figure 3 illustrates the attenuation and dispersion of the nTOF signals as they are transmitted through sequentially longer fiber delays. Comparing the shortest uncorrupted fiber channel (channel 6) to the longest, the signal to noise ratio (SNR) decreases to $\sim 6\%$ of the initial value (from 190 to 11). To check whether an ion temperature can potentially be extracted with degraded SNR,

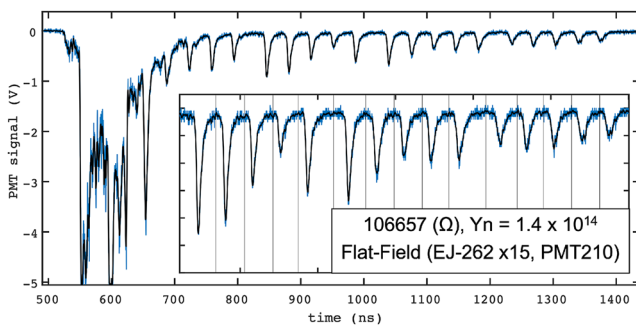


FIG. 3. Multiplexed PMT signal for OMEGA shot 106657 at the lower pylon. The blue trace is raw data, while the black trace is a moving average. The inset illustrates the channels that are not corrupted by early time background.

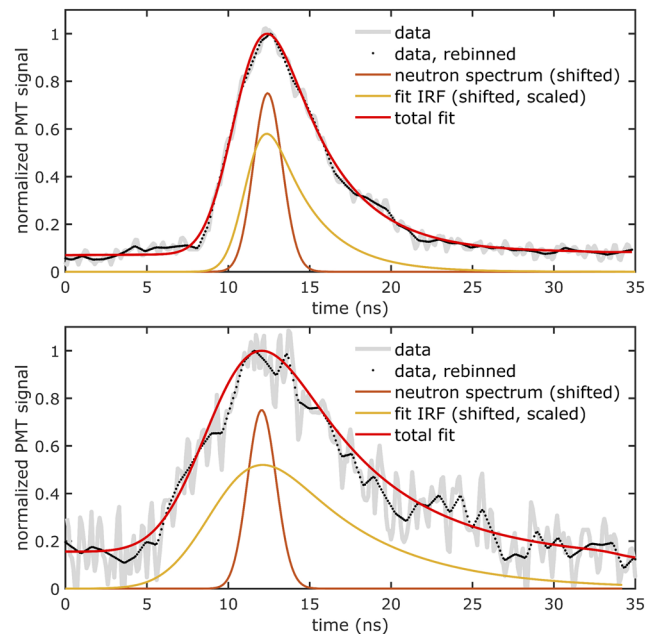


FIG. 4. Fits of the primary DT peak (no scatter component) for the nTOF signals through channels 6 (top) and 20 (bottom) using inferred IRFs calibrated to $\langle T_{ion} \rangle = 12$ keV from the 13 m nTOF.

the forward-fit described in Sec. I was attempted, assuming minimal attenuation and uniform spectral response in the scintillator.

The detector response $R(t)$ is unique to each fiber channel and is currently still being measured. An alternative approach to compare the signals, given that the goal of this experiment is only to probe how well the multiplexed signals can be forward-fit to the same neutron spectrum, is to calibrate the data to the fixed nTOF detectors at OMEGA. The expected value for $\langle T_{ion} \rangle$ is known from the fixed nTOFs and can be used to infer the combined IRF and fiber response, assuming the exponential Gaussian form discussed in Sec. I. Fits used to infer the IRF based on the ion temperature measured by the fixed nTOF suite are shown in Fig. 4 for the shortest and longest fiber channels. The fits shown model the combined IRF as a Gaussian convolved with a single exponential decay component, but results are consistent when including more decay constants.

Consistent fits are obtained between all fiber channels using this calibration. Qualitatively, the combined IRF FWHM increases with fiber length, as expected due to the dispersion component, but the increase is less than analytically estimated. This may be due to charge build-up in the MCPs from the early time signal, which is discussed at the end of this section and has been mitigated in follow-on experiments. If the IRF inferred from this technique were to be well-calibrated to the fixed nTOFs and assumed to be the known response, reversing the fit should converge to the starting ion temperature. From this, a qualitative statistical uncertainty could be calculated from the covariance matrix. For these data, the relative statistical uncertainty on the ion temperature parameter is found to increase from 0.2 keV at the shortest fiber to 0.6 keV at the longest, which qualitatively compares the signal degradation. It is important

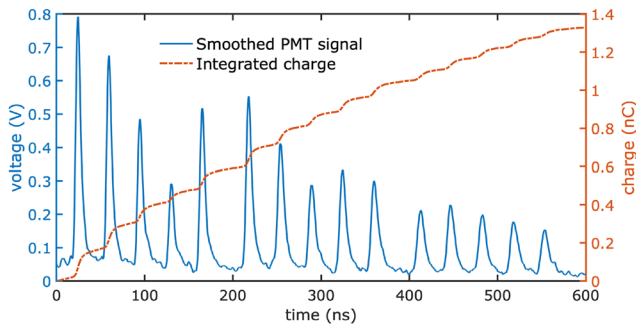


FIG. 5. Integrated charge on the PMT (positioned at the lower pylon) from the nTOF pulse train only. The saturation limit is reached near channel 17 due to higher signal pulses from the short fibers.

to note that this does not capture the systematic uncertainties of a measured IRF that may dominate in a full detector.

Although consistent fits are obtained for all channels, the technique is sensitive to SNR reduction and dispersion. The minimum fiber length to avoid the early time background is found to be around 100 ft for the OMEGA lower pylon. As this multiplexer was an initial proof-of-concept designed only to demonstrate the technique, follow-on designs will utilize larger core silica fibers, an optimized PMT mount to improve coupling efficiency, larger delay lengths, and more fibers per scintillator to increase carrier statistics. Graded-index fibers could be used to reduce modal dispersion, which appears to dominate the IRF difference between fiber channels, but may not be compatible with the scintillator emission spectrum.

Another limiting factor in the number of fiber channels and delay lengths is charge saturation of the PMT, which occurs at ~ 1.2 nC for the PMT210.²⁴ The early time signal of fast fusion products introduces significant charge build-up that saturates the PMT before the neutron signals of interest even arrive. As such, the PMT MCPs need to be gated off prior to the arrival time of the first neutron pulse. This has been demonstrated in several experiments following that shown in Fig. 3 using a Photek GM300-3P MCP gate module, but analysis of these data is still in progress.

Given that charge recovery in the MCPs is not expected to occur on timescales shorter than the nTOF pulse train, the integrated charge from the multiplexed signals needs to stay below the saturation limit as well. Integrated charge as a function of time for just the nTOF pulses in Fig. 3 is shown in Fig. 5. To operate the PMT near maximum gain in a future detector, optical attenuators can be implemented on shorter fibers to extend the available charge and accommodate more nTOF pulses. In scaling up to a full system, a larger PMT could also be used (e.g., PMT240) to increase the charge saturation limit.

V. SUMMARY AND OUTLOOK

Spatially resolved nTOF diagnostics of ICF implosions can be achieved by strategically combining techniques in neutron imaging with neutron time-of-flight. A 1D system has already been demonstrated, and a 2D concept is currently being designed to reconstruct

the ion temperature spatial distribution from multiple 1D projections. Such a design is feasible if the 1D nTOF is modified to use a PMT, which can be achieved, in principle, by time-multiplexing signals from separate scintillators using optical fiber delays. Ride-along experiments on OMEGA calibrated to fixed nTOF detectors suggest that multiplexing can potentially preserve features of the neutron time spectrum necessary to extract the ion temperature, but further study of the IRF and dispersion linearity is required to quantify the uncertainties. Results emphasize that the design of multiplexed nTOF detectors is dominated by coupling efficiencies, optical fiber attenuation and dispersion, and charge collection in the PMT MCPs. IRF measurement and analysis of unsaturated results with a spatially resolved multiplexed detector will be discussed in future work.

Although time-multiplexing is described herein in the context of adding spatial resolution to an nTOF detector, the viability of multiplexed nTOF would have implications for several other applications as well. Such applications for scintillation detectors may include dynamic range modification, multi-scintillator geometries (e.g., sampling the nTOF spectrum at different distances and/or angles with a single PMT), background discrimination, and more.

ACKNOWLEDGMENTS

The authors would like to acknowledge Brandon Aguirre, Hermann Geppert-Kleinrath, and Zarah Mohamed for supporting this diagnostic in their campaigns at OMEGA. This work was performed for the National Nuclear Security Administration under the auspices of the U.S. Department of Energy by the Los Alamos National Laboratory under Contract No. 89233218CNA000001. This work was also supported by the National Science Foundation Graduate Research Fellowship under Grant No. DGE-224114 and by the Center for Magnetic Acceleration, Compression, and Heating (MACH), part of the NNSA Stewardship Science Academic Alliances program, under DOE Cooperative Agreement No. DE-NA0004148.

AUTHOR DECLARATIONS

Conflict of Interest

The authors have no conflicts to disclose.

Author Contributions

L. Tafoya: Formal analysis (lead); Investigation (lead); Methodology (lead); Visualization (lead); Writing – original draft (lead). **C. Wilde:** Conceptualization (lead); Formal analysis (equal); Investigation (lead); Methodology (lead); Supervision (equal); Writing – review & editing (equal). **B. Cata:** Resources (equal). **M. Freeman:** Investigation (equal); Writing – review & editing (equal). **V. Geppert-Kleinrath:** Formal analysis (supporting); Project administration (supporting). **S. Ivancic:** Investigation (supporting); Resources (supporting). **J. Katz:** Investigation (supporting); Resources (equal). **R. McBride:** Resources (supporting); Writing – review & editing (equal). **A. Sorce:** Investigation (supporting); Resources (supporting). **B. Stanley:** Investigation (equal); Resources (supporting); Writing – review & editing (equal). **C. Danly:** Conceptualization

(equal); Formal analysis (equal); Investigation (lead); Methodology (lead); Supervision (lead); Writing – review & editing (equal).

DATA AVAILABILITY

The data that support this study are available from the corresponding author upon reasonable request and security review.

REFERENCES

- ¹R. Betti and O. Hurricane, “Inertial-confinement fusion with lasers,” *Nat. Phys.* **12**, 435–448 (2016).
- ²H. Abu-Shawareb *et al.*, “Lawson criterion for ignition exceeded in an inertial fusion experiment,” *Phys. Rev. Lett.* **129**, 075001 (2022).
- ³T. Ma, P. K. Patel, N. Izumi *et al.*, “Onset of hydrodynamic mix in high-velocity, highly compressed inertial confinement fusion implosions,” *Phys. Rev. Lett.* **111**, 085004 (2013).
- ⁴S. P. Regan, R. Epstein *et al.*, “Hot-spot mix in ignition-scale inertial confinement fusion targets,” *Phys. Rev. Lett.* **111**, 045001 (2013).
- ⁵B. M. Haines, R. C. Shah, J. M. Smidt *et al.*, “The rate of development of atomic mixing and temperature equilibration in inertial confinement fusion implosions,” *Phys. Plasmas* **27**, 102701 (2020).
- ⁶H. Brysk, “Fusion neutron energies and spectra,” *Plasma Phys.* **15**, 611 (1973).
- ⁷L. Ballabio, J. Källne, and G. Gorini, “Relativistic calculation of fusion product spectra for thermonuclear plasmas,” *Nucl. Fusion* **38**, 1723 (1998).
- ⁸D. H. Munro, “Interpreting inertial fusion neutron spectra,” *Nucl. Fusion* **56**, 036001 (2016).
- ⁹C. J. Forrest, P. B. Radha, V. Y. Glebov *et al.*, “High-resolution spectroscopy used to measure inertial confinement fusion neutron spectra on omega (invited),” *Rev. Sci. Instrum.* **83**, 10D919 (2012).
- ¹⁰A. S. Moore, E. P. Hartouni, D. Schlossberg *et al.*, “The five line-of-sight neutron time-of-flight (nToF) suite on the National Ignition Facility (NIF),” *Rev. Sci. Instrum.* **92**, 023516 (2021).
- ¹¹G. A. Chandler *et al.*, “Neutron time-of-flight detectors (nTOF) used at Sandia’s Z-machine,” *Rev. Sci. Instrum.* **93**, 113531 (2022).
- ¹²A. S. Moore, D. J. Schlossberg, B. D. Appelbe *et al.*, “Neutron time of flight (nToF) detectors for inertial fusion experiments,” *Rev. Sci. Instrum.* **94**, 061102 (2023).
- ¹³R. Hatarik, D. B. Sayre, J. A. Caggiano *et al.*, “Analysis of the neutron time-of-flight spectra from inertial confinement fusion experiments,” *J. Appl. Phys.* **118**, 184502 (2015).
- ¹⁴D. J. Morrow and X. Ma, “Rapid and facile reconstruction of time-resolved fluorescence data with exponentially modified Gaussians,” [arXiv:2201.03561](https://arxiv.org/abs/2201.03561) [physics.data-an] (2023).
- ¹⁵D. N. Fittinghoff, N. Birge, and V. Geppert-Kleinrath, “Neutron imaging of inertial confinement fusion implosions,” *Rev. Sci. Instrum.* **94**, 021101 (2023).
- ¹⁶C. Danly, N. Birge, V. Geppert-Kleinrath *et al.*, “Modeling of a spatially resolved ion temperature diagnostic for inertial confinement fusion,” *Rev. Sci. Instrum.* **94**, 043502 (2023).
- ¹⁷N. Birge, V. Geppert-Kleinrath, C. Danly *et al.*, “Instrument design for an inertial confinement fusion ion temperature imager,” *Rev. Sci. Instrum.* **93**, 113510 (2022).
- ¹⁸P. L. Volegov, C. R. Danly, F. E. Merrill *et al.*, “On three-dimensional reconstruction of a neutron/x-ray source from very few two-dimensional projections,” *J. Appl. Phys.* **118**, 205903 (2015).
- ¹⁹M. Bangert, “CT reconstruction package,” MATLAB Central File Exchange (2024) <https://www.mathworks.com/matlabcentral/fileexchange/34608-ct-reconstruction-package>
- ²⁰K. Cochrane, J. E. Bailey, P. Lake, and A. Carlson, “Wavelength-dependent measurements of optical-fiber transit time, material dispersion, and attenuation,” *Appl. Opt.* **40**, 150–156 (2001).
- ²¹T. Ecker, D. Brooks, and K. Lowe, “Development and application of a point Doppler velocimeter featuring two-beam multiplexing for time-resolved measurements of high-speed flow,” *Exp. Fluids* **55**, 1819 (2014).
- ²²B. V. Beeman, A. C. Carpenter, J. R. Kimbrough *et al.*, “Mach-Zehnder detector system issues and enhancements for use on the National Ignition Facility DANTE x-ray diagnostic,” *SPIE Proc.* **9211**, 92110E (2014).
- ²³E. Hecht, *Optics*, 4th ed. (Pearson, 2002).
- ²⁴J. S. Milnes, T. M. Conneely, and C. J. Horsfield, *Rev. Sci. Instrum.* **87**, 11D832 (2016).